J Biol Inorg Chem
DOI 10.1007/s00775-016-1433-0

ORIGINAL PAPER

Inhibition of copper-mediated aggregation of human γD-crystallin by Schiff bases

Priyanka Chauhan[1] · Sai Brinda Muralidharan[2] · Anand Babu Velappan[2] · Dhrubajyoti Datta[3] · Sanjay Pratihar[4] · Joy Debnath[2] · Kalyan Sundar Ghosh[1]

Received: 30 August 2016 / Accepted: 13 December 2016

Abstract Protein aggregation, due to the imbalance in the concentration of Cu^{2+} and Zn^{2+} ions is found to be allied with various physiological disorders. Copper is known to promote the oxidative damage of β/γ-crystallins in aged eye lens and causes their aggregation leading to cataract. Therefore, synthesis of a small-molecule 'chelator' for Cu^{2+} with complementary antioxidant effect will find potential applications against aggregation of β/γ-crystallins. In this paper, we have reported the synthesis of different Schiff bases and studied their Cu^{2+} complexation ability (using UV–Vis, FT-IR and ESI-MS) and antioxidant activity. Further based on their copper complexation efficiency, Schiff bases were used to inhibit Cu^{2+}-mediated aggregation of recombinant human γD-crystallin (HGD) and β/γ-crystallins (isolated from cataractous human eye lens). Among these synthesized molecules, compound **8** at a concentration of 100 μM had shown ~95% inhibition of copper (100 μM)-induced aggregation. Compound **8** also showed a positive cooperative effect at a concentration of 5–15 μM on the inhibitory activity of human αA-crystallin (HAA) during Cu^{2+}-induced aggregation of HGD. It eventually inhibited the aggregation process by additional ~20%. However, ~50% inhibition of copper-mediated aggregation of β/γ-crystallins (isolated from cataractous human eye lens) was recorded by compound **8** (100 μM). Although the reductive aminated products of the imines showed better antioxidant activity due to their lower copper complexing ability, they were found to be non-effective against Cu^{2+}-mediated aggregation of HGD.

Graphical Abstract

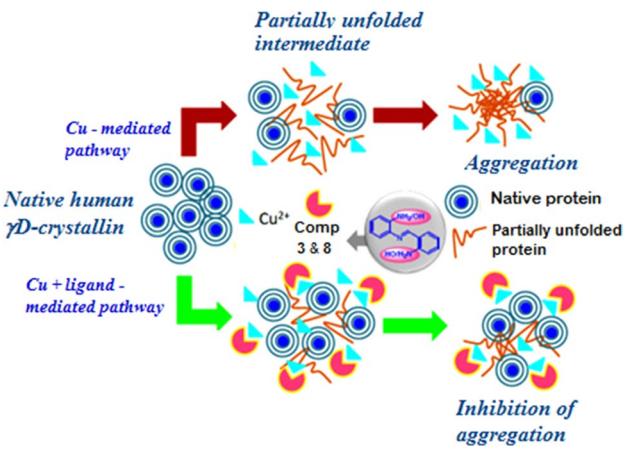

Keywords Schiff base · Copper complex · γ-Crystallin · α-Crystallin · Cu^{2+}-induced aggregation inhibition

Electronic supplementary material The online version of this article (doi:10.1007/s00775-016-1433-0) contains supplementary material, which is available to authorized users.

✉ Joy Debnath
joydebnath@scbt.sastra.edu

✉ Kalyan Sundar Ghosh
kalyan@nith.ac.in

[1] Department of Chemistry, National Institute of Technology Hamirpur, Hamirpur, Himachal Pradesh 177005, India

[2] Department of Chemistry, School of Chemical and Biotechnology, SASTRA University, Thanjavur, Tamilnadu 613401, India

[3] Department of Chemistry, Indian Institute of Science Education and Research Pune, Pune, Maharashtra 411008, India

[4] Department of Chemical Sciences, Tezpur University, Tezpur 784 028, India

Published online: 05 January 2017

Introduction

Some metal ions, especially Cu^{2+} and Zn^{2+} have been found to be involved in the process of protein aggregation and can eventually cause different neurodegenerative disorders like Alzheimer's, Parkinson's disease, etc. [1–3]. Dyshomeostasis of these metal ions leads to the Aβ aggregation and subsequent neurotoxicity in Alzheimer's disease along with the formation of reactive oxygen species (ROS) [4–6]. Although the specific mechanism of metal-induced aggregation is not very clear, the generation of oxidative stress by the metal ions during aggregation has been well documented in literature [7, 8]. Similarly, metal-catalyzed oxidation of eye lens crystallin proteins causes their aggregation and results in cataract [9–12], a leading cause of blindness. Three major types of crystallins (α-, β- and γ-) are present in the eye lens and there is no turnover of these proteins in the aged fiber cells of the lens. Generally due to the aggregation of β- and γ-crystallins, light scattering elements are produced and hence increase the opacity of the lens. In addition to that, the aggregates once formed will remain for rest of the life of an individual due to the lack of methods to remove the aggregated proteins from lens. At present, there is almost no other alternative to the cataract treatment except eye surgery. Hence, the development of pharmaceuticals that can inhibit or even slow down the aggregation process will have remarkable impact and by that a significant amount of medical cost could be saved.

Copper is present in a tightly bound form with the crystallins in normal eye lens and this tight binding suppresses Cu^{2+}-mediated ROS generation in the lens [13]. Alpha-crystallin (small heat shock protein in the lens) is also involved in sequestration of Cu^{2+} ion present in lens to exhibit its cytoprotective effects against oxidation [14]. In addition, the binding of Cu^{2+} and Zn^{2+} with α-crystallins causes an increase in their chaperone activity [15, 16]. But with ageing of the lens, α-crystallins as molecular chaperone start to form stable complexes with their natural substrate β/γ-crystallins and prevent their aggregation [17, 18]. It has also been reported that the binding of β- and γ-crystallin to α-crystallin decreases its Cu^{2+}-binding capability [19]. Therefore, with increase in the age of an individual, the amount of free α-crystallin as well as its chaperone activity is significantly compromised. This should indeed increase the concentration of free copper ion in the cataractous lens [20–22] and can create oxidative insults for β/γ-crystallins. A recent study has confirmed Cu^{2+} and Zn^{2+} induced rapid aggregation of HGD leads to the formation of light scattering aggregates [23]. So the sequestration of copper ions by small molecules would be a promising strategy against this situation to prevent further oxidative damage and aggregation of β/γ-crystallins.

In the earlier reports on regulation of metal-induced protein aggregation, it was found that 8-hydroxyquinoline derivatives can significantly inhibit metal-mediated aggregation of Aβ peptide [24, 25]. 8-Hydroxyquinoline conjugated with cyclodextrin showed anti-aggregation efficiency against metal-induced aggregation of β-lactoglobulin [26]. Several bifunctional small molecules can also control the metal-induced aggregation of Aβ peptide [27, 28]. It is also reported that 8-hydroxyquinoline Schiff base compounds can act as antioxidants and modulate Cu^{2+}-mediated Aβ peptide aggregation [29]. Some of these metal chelators are in the process of clinical trials against neurodegenerative disorders. Among them, clioquinol (chelating agent of copper and zinc) can also dissolve the amyloid deposits in vitro and in vivo, which were generated due to copper and zinc dyshomeostasis [25]. This compound was also used successfully against the Parkinson's disease, where it reduces the oxidation and amyloid burden [30]. Another derivative of 8-hydroxyquinoline, e.g., (5, 7-dichloro-2-[(dimethylamino)-methyl-8-hydroxyquinoline] (PBT2) has also been successfully completed the phase II trial for the Alzheimer's (http://clinicaltrials.gov) and mouse model for the Huntington's disease [31].

In this study, we have designed and synthesized a series of Schiff bases (metal chelator) to inhibit Cu^{2+}-mediated aggregation of human γD-crystallin (HGD). The major reasons behind the selection of these Schiff bases are their architectural flexibility, ease of their synthesis and their ability to form stable complex with Cu^{2+}. In fact, the π-electron donating capability of the imine nitrogen atom in these ligands would have a great contribution in the formation of stable complexes with transition metals. Additionally, the antioxidant activity of Schiff bases [29, 32, 33] may also protect the proteins from Cu^{2+}-induced oxidative damage. Therefore, the Schiff bases having suitable functional groups can be used against copper-induced protein aggregation by virtue of their synergistic effects of the metal complexation and antioxidant activity. To get a further insight about the role of imine group in aggregation inhibition, the reduced analogues of these Schiff bases were synthesized and tested.

Materials and methods

Synthesis of compounds

Two different sets of compounds have been prepared for comparison of their complexing ability with Cu^{2+} and their relative antioxidant activity. The first set contains the Schiff bases and the second set of compounds was synthesized by the reductive amination of the Schiff bases (Scheme 1).

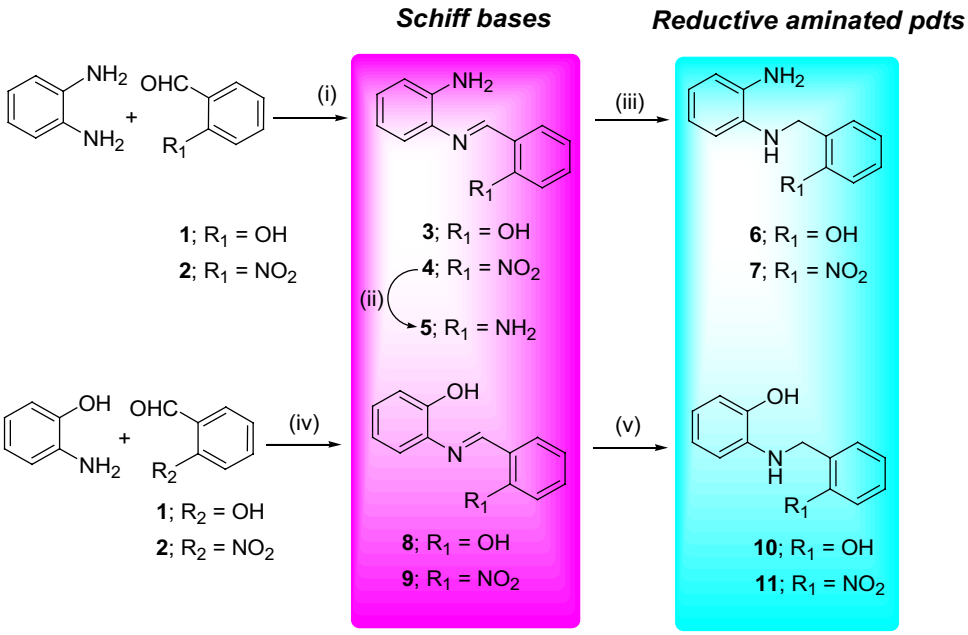

Scheme 1 Synthesis of ligand molecules **3**–**11**. Reagents and reaction conditions: *i* crushing in a mortar and pestle, rt, 5 min; *ii* $Na_2S{\cdot}H_2O$ in EtOH, 70 °C, 30 min. *iii* $NaBH_4$ in MeOH, 0 °C-rt, 3 h; *iv* acetic acid (cat.) in methanol, rt-reflux, 1–3 h; *v* $NaBH_3CN$/AcOH (cat.) in DCM, 0 °C-rt, overnight

Compound ***3*** The *o*-phenylenediamine (0.50 g, 4.6 mmol) was crushed in a mortar pestle followed by the addition of salicylaldehyde (0.5 ml, 4.6 mmol). These two components were then mixed together at room temperature for 5 min (TLC). The solid thus obtained was purified over the silica gel column to yield compound **3** (0.903 g, 92%). Color: yellow solid; mp: 108–110 °C; ^{1}H NMR (300 MHz) (DMSO-d_6) δ 6.93 (dt, J = 0.9, 9.0 Hz, 1H), 7.05 (d, J = 8.1 Hz, 1H), 7.26–7.21 (m, 2H), 7.40–7.32 (m, 4H), 8.64 (s, 1H). HRMS (ESI+): *m/z* calcd for $C_{13}H_{13}N_2O$ $[M + H]^+$: 213.1022; found: 213.1020.

Compound ***4*** The *o*-phenylenediamine (0.36 g, 3.30 mmol) was crushed in a mortar pestle followed by the addition of *o*-nitrobenzaldehyde (0.50 g, 3.30 mmol). These two components were then mixed together at room temperature for 5 min (TLC). The solid thus obtained at the end of the reaction was purified over a silica gel column to yield compound **4** (0.76 g, 95%). Color: yellow orange solid; mp: 89–91 °C; FT-IR (KBr): 3447, 3363, 1616 (s), 1518 (s), 1339 (s), 749 (s). ^{1}H NMR (300 MHz) (DMSO-d_6) δ 5.27 (s, 2H, NH_2), 6.55 (t, J = 1.5 Hz, 1H), 6.73 (d, J = 8.1 Hz, 1H), 7.02 (t, J = 7.2 Hz, 1H), 7.11 (d, J = 7.8 Hz, 1H), 7.78 (td, J = 7.8, 33.0 Hz, 1H), 8.05 (d, J = 8.1 Hz, 1H), 8.33 (d, J = 7.8 Hz, 1H), 8.86 (s, 1H). HRMS (ESI+): *m/z* calcd for $C_{13}H_{12}N_3O_2$ $[M + H]^+$: 242.0924; found: 242.0923.

Compound ***5*** It was prepared by selective reduction of the nitro in presence of the imine with the help of $Na_2S{\cdot}H_2O$ [34, 35]. The ethanolic solution (10 ml) of compound **4** (0.17 g, 0.68 mmol) was mixed with sodium sulphide ($Na_2S{\cdot}H_2O$) (0.40 g, 4.1 mmol) and then refluxed for 30 min at 70 °C. After completion of the reaction (TLC) it was quenched with water, and the solid precipitate thus obtained was filtered out and purified through silica gel column to obtain compound **5** (0.13 g, 90%). Color: olive green solid; mp: 118–120 °C; FT-IR (KBr): 3445 (s), 3369 (s), 3286 (s), 1615 (s), 1487, 744 (s). ^{1}H NMR (300 MHz) ($CDCl_3$) δ 6.82–6.71 (m, 4H), 6.97 (dd, J = 1.5, 8.1 Hz, 1H), 7.09–6.95 (m, 1H), 7.25–7.19 (m, 1H), 7.36 (dd, J = 1.5, 7.8 Hz, 1H), 8.56 (s, 1H). HRMS (ESI+): *m/z* calcd for $C_{13}H_{14}N_3$ $[M + H]^+$: 212.1182; found: 212.1182.

Compound ***6*** The compound **3** (0.20 g, 0.94 mmol) was dissolved in 10 ml of MeOH and the temperature was brought to 0 °C by using an ice bath. To this cold solution, a measured amount of sodium borohydride (0.11 g, 2.82 mmol) was added and stirring was continued for another 3 h at room temperature. After completion of the reaction (TLC), it was quenched by adding water. The compound was then filtered and reprecipitated from hexane and purified through silica column to yield compound **6** (0.18 g, 88%). Color: pale brown solid; mp: 149–151 °C; ^{1}H NMR (300 MHz) ($CDCl_3$) δ 4.41 (s, 2H), 6.94–6.72 (m, 6H), 7.25–7.18 (m, 2H). HRMS (ESI+): *m/z* calcd for $C_{13}H_{15}N_2O$ $[M + H]^+$: 215.1179; found: 215.1176.

Compound ***7*** The compound **4** (0.20 g, 0.89 mmol) was dissolved in 10 ml of MeOH and the temperature was brought to 0 °C by using an ice bath. To this cold solution, a measured amount of sodium borohydride (0.26 g, 4.14 mmol) was added and stirring was continued for another 3 h at room temperature. After completion of the reaction (TLC), it was quenched by adding water. The compound was filtered and reprecipitated from hexane and purified through silica column to yield compound **7** (0.18 g, 90%). Color: orange solid; mp-101–103 °C; FT-IR (KBr): 3392, 1595,

1508 (s), 1335 (s), 744 (s). ^{1}H NMR (300 MHz) ($CDCl_3$) δ 4.71 (s, 2H), 6.48 (dd, J = 5.4, 7.5 Hz, 1H), 6.68–6.78 (m, 3H), 7.02 (t, J = 7.2 Hz, 1H), 7.43 (t, J = 6.9 Hz, 1H), 7.53–7.62 (m, 2H), 8.05 (d, J = 6.9 Hz, 1H). HRMS (ESI+): *m/z* calcd for $C_{13}H_{14}N_3O_2$ $[M + H]^+$: 244.1081; found: 244.1079.

Compound ***8*** Salicylaldehyde (0.52 g, 4.26 mmol) was dissolved in methanol (10 ml) and stirred at room temperature for 5 min followed by the slow addition of 2-aminophenol (0.46 g, 4.26 mmol). It was then stirred at room temperature for 1 h. Then the methanol was removed under reduced pressure and the organic portion was extracted with ethyl acetate (50 ml × 3). Finally, the organic layer was washed with water and brine and dried over sodium sulphate followed by the concentration under reduced pressure. The crude residue thus obtained was purified by column chromatography to afford compound **8** (0.81 g, 89.3%). Color: dark orange solid; mp: 189–191 °C; ^{1}H NMR (300 MHz) ($CDCl_3$) δ 6.97–7.06 (m, 4H), 7.15 (d, J = 5.4 Hz, 1H), 7.21–7.26 (m, 1H), 7.40–7045 (m, 2H), 8.69 (s, 1H). HRMS (ESI+): *m/z* calcd for $C_{13}H_{12}NO_2$ $[M + H]^+$: 214.0863; found: 214.0866.

Compound ***9*** 2-Aminophenol (0.4 g, 3.67 mmol) was dissolved in methanol (10 ml) followed by the addition of 2-nitrobenzaldehyde (0.55 g, 3.67 mmol) and catalytic amount of acetic acid. The reaction mixture was then refluxed for 3 h. Thereafter, the methanol was removed under reduced pressure and the crude thus obtained was crystallized from ethylacetate to yield compound **9** (0.74 g, 83.8%). Color: greenish yellow colored solid; mp-109–111 °C; FT-IR (KBr): 3378, 1519 (s), 1339 (s), 1228 (s), 752 (s). ^{1}H NMR (300 MHz) ($CDCl_3$) δ 6.95–6.92 (m, 1H), 7.04–7.02 (m, 1H), 7.36–7.24 (m, 2H), 7.64 (t, J = 5.7 Hz, 1H), 7.75 (t, J = 5.7 Hz, 1H), 8.06 (d, J = 6.0 Hz, 1H), 8.26 (d, J = 6.0 Hz, 1H), 9.17 (s, 1H). HRMS (ESI+): *m/z* calcd for $C_{13}H_{11}N_2O_3$ $[M + H]^+$: 243.0764; found: 243.0760.

Compound ***10*** The compound **8** (0.50 g, 2.3 mmol) was dissolved in 5 ml of DCM and 0.5 ml of acetic acid and the temperature was then brought to 0 °C by using an ice bath. To this cold solution, a measured amount of $NaBH_3CN$ (0.29 g, 4.2 mmol) was added and stirring was continued for another 1 h at room temperature. After completion of the reaction (TLC), it was quenched by adding water and extracted with chloroform (2 times). The combined organic layers were then concentrated under reduced pressure and purified through silica gel column to afford comp 10 (0.44 g, 88%). Color: brown solid; mp: 99–101 °C; ^{1}H NMR (300 MHz) ($CDCl_3$) δ 4.41 (s, 2H), 6.91–6.72 (m, 6H), 7.25–7.15 (m, 2H). HRMS (ESI+): *m/z* calcd for $C_{13}H_{14}NO_2$ $[M + H]^+$: 216.1019; found: 216.1020.

Compound ***11*** The compound **9** (0.20 g, 8.1 mmol) was dissolved in 5 ml of DCM and 0.5 ml of acetic acid and the temperature was then brought to 0 °C using an ice bath. To this cold solution, a measured amount of $NaBH_3CN$ (0.94 g, 24.3 mmol) was added and stirring was continued for another 1 h at room temperature. After completion of the reaction (TLC), it was quenched by adding water and extracted by chloroform (2 times). The combined organic layers were then concentrated under reduced pressure and purified through silica gel column to afford comp 10 (0.17 g, 85%). Color: brown liquid; FT-IR (KBr): 3405, 1611, 1521 (s), 1342 (s), 729 (s). ^{1}H NMR (300 MHz) ($CDCl_3$) δ 4.74 (s, 2H), 6.46 (d, J = 7.8 Hz, 1H), 6.64 (t, J = 7.2 Hz, 1H), 6.76 (d, J = 7.2 Hz, 2H), 7.45–7.40 (m, 1H), 7.60–7.54 (m, 1H), 7.67–7.4 (m, 1H), 8.08 (dd, J = 1.2, 8.1 Hz, 1H). HRMS (ESI+): *m/z* calcd for $C_{13}H_{13}N_2O_3$ $[M + H]^+$: 245.0921; found: 245.0923.

Complexation studies of the compound 3–11 with Cu^{2+}

For complexation studies, stock solution of the metal ion was prepared by dissolving $CuCl_2$ in water. All the metal–ligand complexations were studied using spectroscopy grade solvents at room temperature.

UV–Vis spectroscopy

The spectra were recorded using a UV–Vis spectrophotometer (Lasany make). For each compound, absorption spectra were collected on successive addition of $CuCl_2$ solution to a solution of that compound in 10 mM phosphate buffer, pH 7.0. The stoichiometry of the respective metal complexes was calculated by mole-ratio method using the Job plot. The absorbance (at a fixed wavelength) upon subsequent addition of Cu^{2+} was plotted against the mole fraction of Cu^{2+}. The stoichiometry was obtained from the breakpoint in that plot. The association constant (K_a) of the copper complex was calculated using the Benesi–Hildebrand equation [36], which was also used elsewhere previously to determine the binding constants of metal–ligand complexes [37–40].

$$\frac{1}{\Delta A} = \frac{1}{\Delta A_{sat}} + \frac{1}{\Delta A_{sat} K_a [Cu^{2+}]}.$$

In the above expression ΔA is the absorbance difference caused on addition of Cu^{2+} to the solution of the ligand at a fixed wavelength and ΔA_{sat} is the maximum absorbance difference at that wavelength. The association constant (K_a) of the copper complexes of the compounds was determined from ratio of the intercept and slope obtained from the plot between the reciprocal of ΔA against the reciprocal of Cu^{2+} concentration.

FT-IR spectroscopy

FT-IR spectra were collected using a Perkin-Elmer spectrophotometer (Model Spectrum RX-IFTIR). The copper

complexes of compounds **8** and **9** were prepared by mixing methanolic solutions of the metal ion and the respective compound at a molar ratio of 1:1 and then the solution was dried to remove methanol. Spectra were collected by making a film of KBr with the metal complex.

Mass spectrometry

High-resolution mass spectrum (HRMS) of the copper complex of compound **8** was recorded using Waters Micromass Q-Tof Micro. The instrument is a hybrid quadrupole time-of-flight mass spectrometer equipped with electrospray ionization (ESI) technique. Before recording the ESI-MS, copper complex of compound **8** was prepared by mixing methanolic solutions of compound **8** and $CuCl_2$ at a molar ratio of 1:1.

Theoretical calculations

All the calculations were performed using Gaussian 09 suite of program [41]. Geometries of the probable copper complexes of compound **8** were optimized at *B3LYP* level of theory employing effective core potential (ECP). The valence basis sets *LANL2DZ* were used for copper and *6-31G** basis set for other atoms. The formation energy of the probable complexes was computed at same level of theory with zero-point energies (ZPE) and thermal corrections at 298 K.

Antioxidant assay

The free-radical scavenging capacity of compounds **3–11** was determined by using 1,1-diphenyl-2-picrylhydrazyl (DPPH) radical decolorization assay as described elsewhere [42]. Briefly, the methanolic solution of the compounds at different concentrations were added to the DPPH solution (~120 μM) in methanol and incubated for 15 min. Then the absorbance of the DPPH alone (control sample) and the DPPH mixed different concentrations of the compound (test samples) were measured at 517 nm. All the solutions were protected from the light during mixing and incubation. The DPPH free-radical scavenging activity was calculated using the following equation. The IC_{50} values for each compound as well as that for ascorbic acid (a common antioxidant) were calculated by the linear regression analysis.

$$\%\text{Radical scavenging activity} = \frac{(\text{Absorbance of control} - \text{absorbance of test sample})}{\text{Absorbance of control}} \times 100$$

Purification of proteins

Expression and purification of HGD

HGD-clone was kindly gifted by Prof. D. Balasubramanian, L.V. Prasad Eye Hospital, Hyderabad, India. The plasmid DNA was transformed into BL21(DE3) competent *E. coli* cells (New England Biolabs). The bacterial cultures were grown at 37 °C in LB Media to an absorbance of ~0.8 at 600 nm. Overexpression of HGD was induced by 1 mM of isopropyl 1-thio-D-galactopyranoside (IPTG). Cultures were then further grown for additional 5 h and bacterial cells were collected by centrifugation. Purification of HGD was done following the method of Pande et al. [43]. Briefly, the cell pellet was lysed in 50 mM Tris–HCl buffer at pH 8.0 containing 25 mM NaCl, 2 mM EDTA, 1 mM each of phenylmethylsulfonyl fluoride (PMSF) and benzamidine hydrochloride in presence of lysozyme (250 μg/ml) using rapid freeze–thaw technique. 50 μl of DNase (Himedia) was then added and incubated for 1 h at room temperature followed by centrifugation. HGD was found mostly in the supernatant, which was subjected to size exclusion (Sephacryl S-200), followed by cation-exchange chromatography (SP-Sepharose). Purity of the protein was checked on an SDS-PAGE gel (SM Fig. S8A). The concentration of HGD was determined by using an extinction coefficient of 2 mM^{-1} cm^{-1} at 280 nm [44].

Expression and purification of HAA

HAA clone was kindly gifted by Prof. K.P. Das, Bose Institute, Kolkata, India. The plasmid DNA was transformed into BL21 (DE3) *E. coli* cells (New England Biolabs) and the bacterial culture was grown at 37 °C till the absorbance of the culture became ~0.8 at 600 nm. Overexpression of HAA was further induced by 1 mM of IPTG and the culture was grown for an additional 5 h. Cells were pelleted by centrifugation. Cell pellets were resuspended in lysis buffer (50 mM Tris–HCl at pH 8.0 containing 25 mM NaCl, 2 mM EDTA, and 1 mM each of PMSF and benzamidine hydrochloride and was lysed with lysozyme (250 μg/ml) followed by five cycles of a rapid freeze and thraw. This cell suspension was incubated with DNase (Himedia) for an hour at room temperature and then it was centrifuged. Both the supernatant and pellet were tested for the presence of HAA using SDS-PAGE and HAA was found mostly in

the supernatant. The supernatant was then loaded to a size exclusion column (Sephacryl S-300 HR) buffered with 0.1 M phosphate buffer of pH 7.0. Three iterations of size exclusion were performed to get the final purified HAA used for further studies. Protein purity was verified using SDS gel electrophoresis (SM Fig. S8B). The concentration of HAA was determined by using an extinction coefficient of 0.83 mM^{-1} cm^{-1} at 280 nm [45].

Purification of β/γ-crystallins from eye lens

Human eye lenses were collected from nearby civil hospital and stored at −80 °C until required. The lenses were homogenized in cold water and the insoluble part was separated by centrifugation (18,000 rpm). The pH of the supernatant was further reduced to 5.0. It was then again centrifuged (18,000 rpm) and the precipitate was discarded following the method of Spector [46]. The soluble β/γ-crystallins fraction (SDS-PAGE shown in SM Fig. S8C) was used for further studies.

Aggregation studies

A solution of HGD or β/γ-crystallins from cataractous lens (~0.3 mg/ml) in 10 mM phosphate buffer (pH 7.0) was mixed with 100 μM Cu^{2+} and then immediately placed in the UV–Vis spectrophotometer. The solution turbidity was measured as the apparent absorbance at 550 nm for an hour time period. Similar set was also run in the presence of the compound (at different concentrations) with the same protein solution under same condition. The cuvette temperature was maintained at 37 °C using a Peltier controller during the experiment. Different concentrations (10–100 μM) of compound **8** were used to study the inhibition of Cu^{2+} (100 μM)-induced aggregation of HGD. Inhibition studies of copper (100 μM)-mediated aggregation of HGD were also carried out individually in presence of other compounds (**3**, **4**, **5**, **9** and **10**) using 100 μM concentration of each. Inhibition of copper-induced aggregation of HGD was also carried out in presence of the different concentrations of HAA alone, using a ratio of HAA:HGD from 0.1:1 to 2:1 under similar experimental conditions. Further, based on our findings, we had used 6.16 μM of HAA and different concentrations of compound **8** (10–30 μM) against Cu^{2+} (100 μM)-induced HGD aggregation to find out its cooperative effect on HAA.

Thioflavin T assay

A solution of β/γ-crystallins (0.1 mg/ml) was mixed with ThT (20 μM) in 10 mM phosphate buffer, pH 7.0 along with 100 μM of Cu^{2+} in absence and presence of 100 μM of compound **8**. The fluorescence emission was recorded using a spectrofluorimeter (Shimadzu RF 5301PC). The excitation and emission wavelengths were set at 440 and 480 nm, respectively.

Results and discussion

To establish the aforementioned concept, Schiff bases were designed in such a way that they can act as bidentate ligand. The Cu^{2+} ion is known to form both five- and six-member ring with a bidentate ligand [47]. Implementation of this information had been carried out for further refinement of the ligand structure, i.e., incorporation of suitable functional groups at the *ortho* position of benzylidene and benzyl moiety.

In this work, we have initially studied the complexation of a series of Schiff bases and their reduced aminated products with Cu^{2+} using multispectroscopic techniques. A major absorption band was found in the range of 350–365 nm for the Schiff bases. This is due to the $\pi \rightarrow \pi^*$ transition in an extended conjugated system involving the aromatic rings and the nitrogen atom of imine. For compound **8**, an additional band was also observed at 436 nm. In the reduced aminated products, due to the loss of that extended conjugation, the same transition was appeared at lower wavelength (275–290 nm).

During complexation, new peaks were generated at 393 and 310 nm with a decrease in absorbance at 351 nm for compound **3** (Fig. 1a). In case of compound **4**, significant development of new absorption band was not observed upon addition of the metal ion (SM Fig. S1A). For compound **5**, generation of new peaks at 469 and 307 nm were recorded along with decrease in absorbance at 364 nm (Fig. 1b); whereas on addition of Cu^{2+}, compound **8** showed an decrease in absorbance at 436 nm with a blue shift and disappearance of the peak at 336 nm (Fig. 1c). However, in case of compound **9**, a new absorption band was developed at 430 nm on addition of Cu^{2+} along with the disappearance of the band at 347 nm (Fig. 1d). The absorption bands of the copper complexes of various ligands appeared at different wavelengths due to the presence of unlike functional groups in the ligands. However, compound **6** (reduced imine) did not show any significant change in the absorption spectra on addition of Cu^{2+} (SM Fig. S1B). For compound **7**, a tiny peak was developed at 394 nm (SM Fig. S1C). In case of compound **10**, formation of a new peak was observed at 400 nm (Fig. 1e) in its copper complex. For compound **11**, only a small hump was found to be developed at 438 nm upon the addition of Cu^{2+} (SM Fig. S1D). The molar stoichiometry of the copper complex of compounds **3**, **5**, **8**, **9** and **10** was calculated from the Job plot (SM Fig. S2) and mentioned in Table 1.

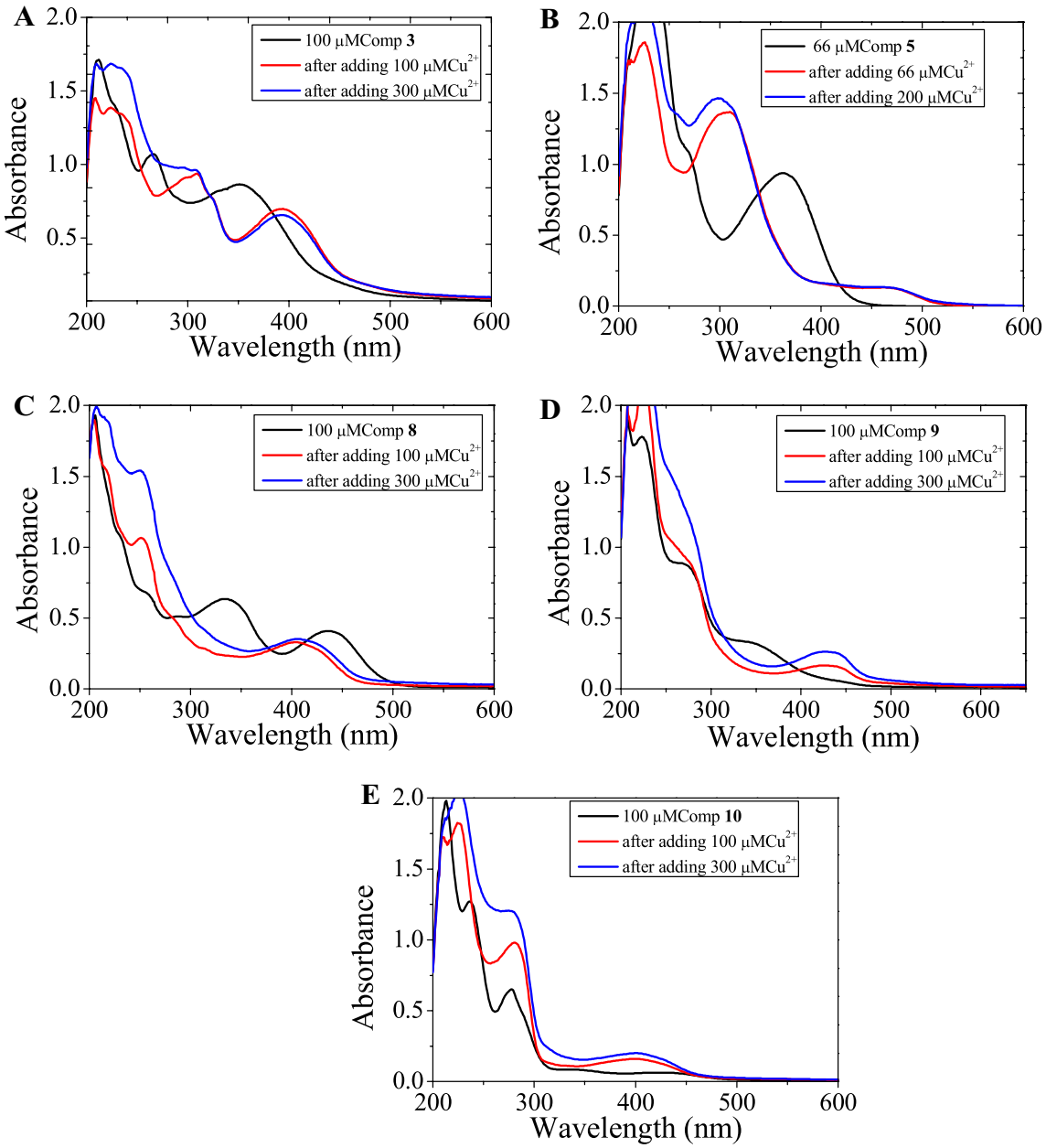

Fig. 1 UV–Vis spectra of the compounds in 10 mM phosphate buffer, pH 7.0 before and after addition of aqueous solution of $CuCl_2$ for **a** compound **3**; **b** compound **5**; **c** compound **8**; **d** compound **9**; and **e** compound **10**. The UV–Vis spectra of the compound only is shown in *black*, while the spectra after addition of one and three molar equivalent of Cu^{2+} is shown in *red* and *blue*, respectively

Table 1 Molar stoichiometry and stability constants of the copper complexes of the compounds

Compound	M:L molar stoichiometry	K_a (M^{-1})
3	1:1	$2.22 \pm 0.14 \times 10^4$
5	1:1	$0.64 \pm 0.03 \times 10^3$
8	1:1	$6.12 \pm 0.31 \times 10^5$
9	1:1	$0.59 \pm 0.05 \times 10^3$
10	1:1	$0.67 \pm 0.03 \times 10^3$

The association constant (K_a) of the copper complexes for compounds **3**, **5**, **8**, **8** and **10** was determined using Benesi–Hildebrand plot (SM Fig. S3) and mentioned in Table 1. Comparison of the stability constants infers the better complexing ability of phenolic –OH group, followed by aromatic $–NH_2$ and aromatic $–NO_2$ groups. The poor association constants of the copper complexes of reduced amines as compared to their respective imines is due to of their capability to form two favorable intramolecular hydrogen bonding, which impeded them to form stable

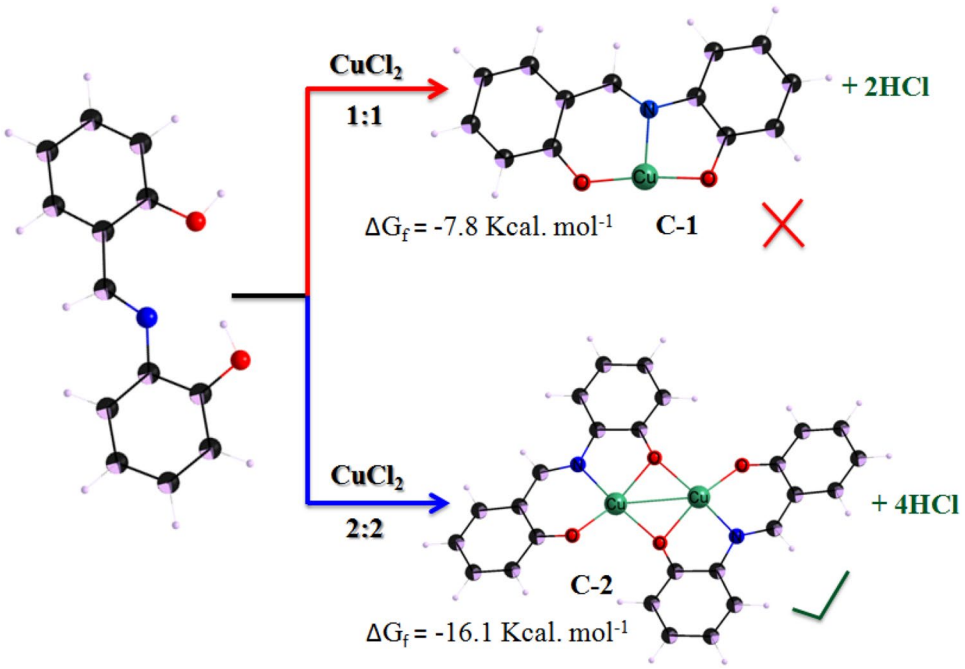

Fig. 2 Probable energy-optimized structures of the Cu^{2+} complex of compound **8**

Table 2 ESI-MS characterization of Cu^{2+}-complex of compound **8**

m/z found in ESI-MS	Relative intensity (%)	Assignment of peak
212.0	47	$[^{b}L–H]^{+}$
213.1	8	$[L]^{+}$
274.2	26	$[^{a}ML–2H]^{+}$
275.0	100	$[ML–H]^{+}$
338.3	8	$[M_2L–H]^{+}$
400.2	42	$[M_3L–2H]^{+}$

[a] M: copper

[b] L: compound **8**

complex with Cu^{2+}. However, in case of imines, only one weak intramolecular hydrogen bonding interaction is possible, which makes them better complexing agent for Cu^{2+} ion as compared to their reduced counterparts (SM Fig. S4).

Among all these compounds, compound **8** was found to form the most stable complex with Cu^{2+}. The copper complex of compound **8** was further characterized in detail. To determine the probable structure of the Cu^{2+} complex of compound **8**, we opt for the energy-optimized calculation after several attempts to crystallize that copper complex were in vain. Based on the binding stoichiometry of 1:1 between copper and ligand (obtained from the Job plot), two probable structures (**C-1** and **C-2**) were optimized at *B3LYP* level of theory using effective core potential (ECP) along with valence basis sets *LANL2DZ* for copper and *6-31G** basis set for other atoms. The energetically most stable structure was determined from free energy difference (ΔG_f) between the product and the reactant with zero-point energies (*ZPE*) and thermal corrections at 298 K. The ΔG_f was found to be more favorable in case of complex C-2, where two copper atoms were bridged between two phenolate groups of ligand and suggested to be more stable as compared to complex C-1 (Fig. 2).

Further, FT-IR spectroscopy was used to investigate the involvement of various functional groups within the metal coordination sphere. The presence of IR bands at 3375, 3304 and 3045–2844 cm^{-1} in compound **8** represents the participation of phenolic –OH in intermolecular and intramolecular hydrogen bonding (SM Fig. S5A). However, the IR spectra of its Cu^{2+} complex showed broadening of the first band and disappearance of the second band. This indicates a significant change of the phenolic–OH environment of the ligand in the copper complex (SM Fig. S5B). Specifically the desertion of the band at 3045–2844 cm^{-1} suggested deprotonation of the phenolic –OH group to form metal–oxygen bond. The migration of the C–O stretching band from 1275–1222 to 1291 cm^{-1} also proved the involvement of the phenolic –OH group in complexation. The coordination through the imine nitrogen was also evident from the shift of imine band from 1632–1592 to 1611–1583 cm^{-1}. The migration of this band to a lower frequency region accounted for the decrease of electron density in the azomethine group due to its involvement in copper complexation. Generation of new bands in the region of 500–400 cm^{-1} also suggested the formation of metal–oxygen and metal–nitrogen bonds in the copper complex. A similar type of behavior was also found in the copper complex of compound **9** (SM Fig. S5C and S5D).

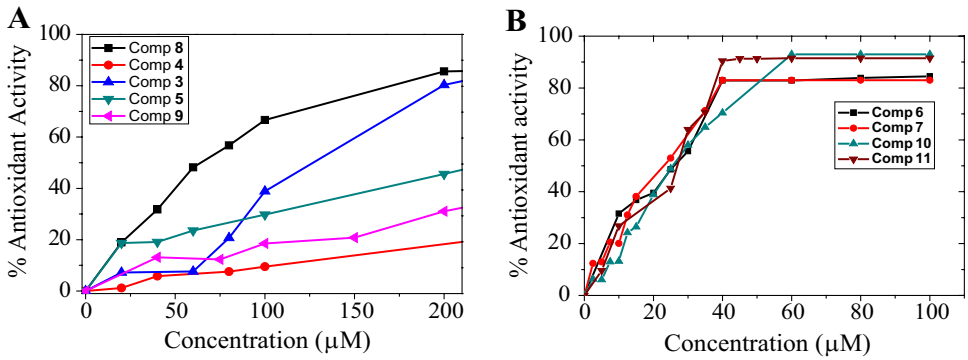

Fig. 3 Antioxidant activity of **a** compounds **3**, **4**, **5**, **8** and **9** and **b** compounds **6**, **7**, **10** and **11** as determined by DPPH method

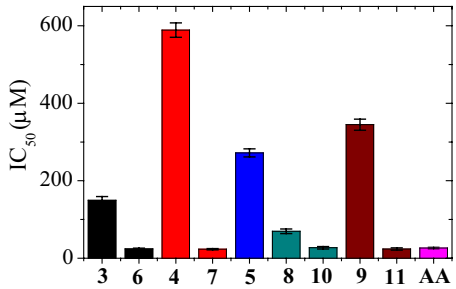

Fig. 4 IC_{50} for the antioxidant activity of the compounds as obtained from DPPH method. *AA* ascorbic acid

Appearance of more than one isosbestic points in the UV–Vis titration spectra (for compound **8**) provided an indication about the presence of different complex species in the solution, which was rigorously determined with the help of ESI-MS spectrometry (SM Fig. S6; Table 2). The ESI-MS findings were suggestive of copper complexation accompanied with the deprotonation of phenolic –OH group. Along with the molecular ion peak of compound **8** (SM Fig. S6), few new peaks were observed due to singly charged metal–ligand complex species like $[ML–H]^+$ and $[ML–2H]^+$, $[M_2L–H]^+$ and $[M_3L–2H]^+$. A distinct molecular ion peak (275.0; with 100% relative intensity) was found for the metal–ligand complex with 1:1 stoichiometry (ML), which unambiguously suggested that the major complex species between Cu^{2+} and compound **8** had the molar stoichiometry of 1:1 and which corroborated well with the results obtained from the Job plot. In addition to this, some metal–ligand complex species having stoichiometries other than 1:1 also appeared. A typical isotopic pattern of the copper complexes was found from the ESI-MS spectrum and it confirmed the existence of metal–ligand complex species like $[ML–H]^+$ and $[M_3L–2H]^+$. The peak for $[ML–H]^+$ and $[ML–2H]^+$ explicitly indicated the involvement of deprotonated phenolic –OH groups of compound **8** in the complexation process.

To find out the efficiency of the synthesized molecules against Cu^{2+}-mediated ROS generation, their antioxidant activity was evaluated. In this assay technique, DPPH can accept an electron or hydrogen radical due to the presence of an odd electron in it. As hydrogen transfer occurs from the antioxidant molecule to DPPH, the absorbance of DPPH decreases at 517 nm. The antioxidant activities of compounds **3–11** as a function of their concentrations are shown in Fig. 3a, b. The corresponding IC_{50} values for the free-radical scavenging capacities of compounds **3–11** are shown in Fig. 4. The IC_{50} for a known antioxidant like ascorbic acid was also determined by the same assay for comparison. Antioxidant potency of the reduced aminated products was found to be same with that of ascorbic acid. It is pertinent to note that the antioxidant activity of compound **8** was the highest among all the imine compounds and also comparable with ascorbic acid because of its two phenolic –OH groups. Lowest antioxidant activity was observed for compound **4** containing an electron-withdrawing nitro group. Among all these compounds, we had found that the compounds containing phenolic –OH group showed better antioxidant activity in DPPH free-radical scavenging (compound **8** vs. **3**, and **9** vs. **4**) due to lower bond dissociation energy of O–H bond than that of N–H bond in this kind of *ortho*-disubstituted aromatic compounds [48, 49]. This is also supported by an earlier report by Bendary et al. [50]. It is reported that the presence of di-active groups in the *ortho* position of a compound is very crucial for its antioxidant efficacy [48, 51, 52]. In this kind of di-substituted structure, the hydrogen atoms (preferentially attached with electronegative oxygen or nitrogen atom) are abstracted followed by the stabilization of the resulting phenoxy radical [52]. A similar kind of molecular scaffold of reduced aminated products explained their higher free-radical scavenging activity compared to their corresponding imine counterpart. This is observed for compounds **6**, **7** (N–H at the *ortho* position of NH_2) and compounds **10** and **11** (N–H at the *ortho* position of OH). The plausible mechanism is shown in SM Fig. S7.

The inhibitory effect of these synthesized compounds against copper-mediated aggregation of HGD was further studied. Notably, compound **8** (20 μM) showed an

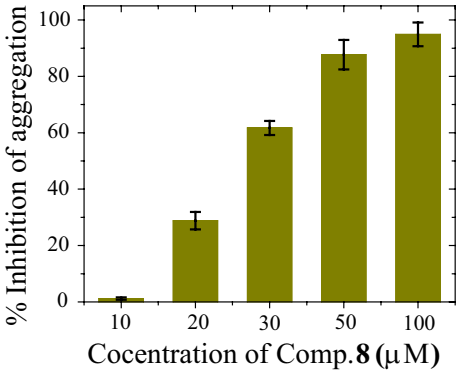

Fig. 5 Percentage inhibition of Cu^{2+} (100 μM)-induced aggregation of HGD (0.5 mg/ml) in 10 mM phosphate buffer, pH 7.0 by different concentrations of compound **8** (10–100 μM). Protein aggregation was monitored by increase in the apparent absorbance at 550 nm due to the increase in the turbidity of HGD solution on addition of Cu^{2+} in absence and presence of the compound

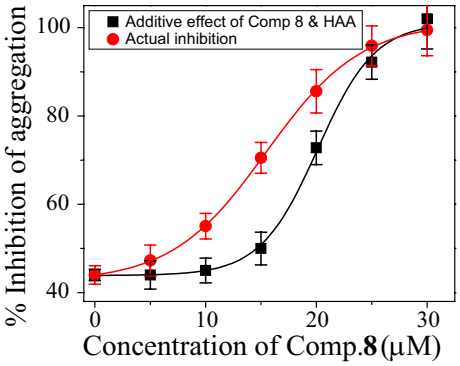

Fig. 6 The positive cooperative effect of compound **8** (at different concentrations) on the inhibitory activity of HAA against copper-mediated aggregation of HGD (~0.5 mg/ml) in 10 mM phosphate buffer, pH 7.0. The concentrations of Cu^{2+} and HAA were 100 and 6.16 μM, respectively. The *black line* represents the additive effect of individual inhibitions done by HAA and compound **8** (at different concentrations) and the *red* one for the actual case

aggregation inhibition of ~29% for HGD in presence of Cu^{2+} (100 μM) and it reached the saturation level (~95%) at 100 μM concentration of compound **8** (Fig. 5). Aggregation inhibition was determined by the apparent change in absorbance at 550 nm. For compound **3**, ~67% aggregation inhibition was recorded at a concentration of 100 μM (SM Fig. S9A). The lower protection efficiency of compound **3** as compared to **8** against copper-mediated aggregation can be attributed to the lower stability constant of the copper complex for compound **3** compared to compound **8**, although the other imines **4** and **9** (100 μM) did not show any inhibition towards HGD aggregation in presence of 100 μM of Cu^{2+} (SM Fig. S9B and S9D). Similarly, we also tested compound **10** (reduced aminated product) to check its inhibitory potential, but it did not show any inhibition of the aggregation process (SM Fig. S9E). For all these molecules, the inhibitory activity against Cu^{2+}-mediated aggregation matches well with the corresponding association constants of their copper complexes. Higher the association constant, lower will be the amount of free Cu^{2+} ions, which can cause the aggregation of HGD. For compound **5**, inhibition of aggregation of HGD was noticed only up to ~20 min in the temporal study (SM Fig. S9C). After that, light scattering was enhanced significantly, which may be due to the breakdown of the metal complex (lower stability) and subsequent release of Cu^{2+} ions from its complex in presence of HGD. Better inhibitory activity of compound **8** compared to **3**, **4**, **5** and **9** can be attributed to the presence of two phenolic –OH groups and these groups remain non-protonated unlike the $–NH_2$ group with significantly high pK_a value. This experimental data clearly demonstrated that in vitro inhibition of Cu^{2+}-mediated aggregation is primarily dependent on the copper complexing ability of the molecule and not on the antioxidant activity.

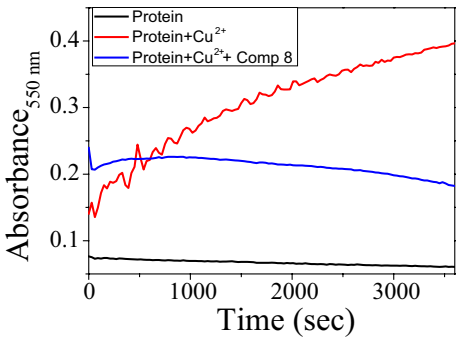

Fig. 7 Time evolution of the turbidity of a solution of β/γ-crystallins (0.25 mg/ml) and Cu^{2+} (100 μM) in absence (*red*) and presence (*blue*) of 100 μM of compound **8**

On the other hand, HAA is known for its chaperon activity and is largely responsible for protection of β- and γ-crystallins from their aggregation in lens. It is also reported that human αB-crystallin can suppress HGD aggregation promoted by Cu^{2+} [23]. Therefore, to find out the effect of compound **8** on the aggregation inhibition by HAA, we had studied the aggregation of HGD with varying concentrations of compound **8** in presence of a fixed concentration of HAA (6.16 μM). At this particular concentration (6.16 μM) of HAA, only ~44% aggregation inhibition was recorded. Nevertheless, the inhibition was found to be increased by ~11% in the presence of compound **8** (10 μM). However, at this particular concentration (10 μM), compound **8** alone showed only ~1% aggregation inhibition of HGD. Thus, the extended inhibitory activity of HAA in presence of the compound **8** eloquently proved its positive cooperative effect. This cooperative effect was

found only at the lower concentration of compound **8** and diminished with the increasing concentration of the compound **8** (Fig. 6). This finding implies that compound **8** is not only able to inhibit the protein aggregation process through direct complexation with Cu^{2+}, but also able to enhance the chaperone activity of HAA leading to better aggregation inhibition than HAA alone.

To ascertain the protective role of compound **8** on a real system, the purified β/γ-crystallins from cataractous human eye lens were used for the aggregation studies in presence of Cu^{2+}. The turbidity of the solutions was monitored at 550 nm as a function of time as mentioned previously. The apparent absorbance (at 550 nm) of a solution containing β/γ-crystallins was found to be increased in the presence of 100 μM Cu^{2+} due to the aggregation and then plateaued out. A reduction in turbidity was observed in presence of the compound **8**, which suggested its inhibitory effect towards metal-induced aggregation of β/γ-crystallins. In presence of the compound **8**, ~50% aggregation inhibition was recorded at 100 μM concentration (Fig. 7). Compound **8** was found to be less protective against Cu^{2+}-induced aggregation of β/γ-crystallins as compared to the recombinant HGD. This can be attributed to various posttranslational modifications that already occurred in the β/γ-crystallins (isolated from cataractous eye lens). However, despite of the reduced activity, this experimental data clearly showed the beneficial role of the Schiff bases against Cu^{2+}-induced aggregation of β/γ-crystallins at the onset of the cataract formation without involving the HAA.

We had also investigated the fibrillogenic nature of the β/γ-crystallins aggregate formed due to the addition of Cu^{2+} using thioflavin T (ThT) fluorescence assay. The fluorescence emission intensity of ThT at 480 nm will be increased if it interacts with amyloids. Therefore, we measured the emission fluorescence intensity of ThT at 480 nm in presence of the β/γ-crystallins (0.1 mg/ml) and 100 μM of Cu^{2+} at pH 7.0. Very weak fluorescence emission intensity of ThT at 480 nm suggested that the aggregate was mostly amorphous rather than amyloid fibril type (SM Fig. S10), which is in agreement with the observation reported earlier [23], and it resembled the common aggregation pattern frequently observed in the eye lens.

Conclusion

Aggregation of β/γ-crystallins is the main reason of cataract formation in eye lens. Dyshomeostasis of copper and zinc in the aged eye lens is one of the important factors which leads to the aggregation of β/γ-crystallin proteins. Therefore, chelation of these metal ions can provide a possible means to protect the β/γ-crystallins from metal-induced aggregation. Schiff bases are well-known chelators of Cu^{2+} ion with complementary antioxidant activity. This study showed that the stability of the Cu–ligand complexes were dependent on the various functional groups present in their corresponding Schiff bases. The phenolic hydroxyl group was found to play an important role for the formation of stable Cu^{2+} complex. The change of IR absorption band and the existence of the $[ML–H]^+$ and $[ML–2H]^+$ peaks in ESI-MS spectra also authenticated the important role of phenolic hydroxyl group during complexation. The Schiff base (compound **8**) with two phenolic hydroxyl groups inhibited the aggregation of HGD up to 95% in presence of Cu^{2+}. However, other compounds **3**, **4**, **5** and **9** showed moderate to no inhibitory activity against Cu^{2+}-induced aggregation of HGD. This finding clearly showed the precedence of the complexing ability over the antioxidant activity. Furthermore, compound **8** also showed ~50% inhibition against the aggregation of β/γ-crystallins purified and isolated from cataractous human eye lens in the presence of Cu^{2+}.

These new findings implemented the potential protective role of the Schiff base against the aggregation process during dyshomeostasis of the Cu^{2+} ion and also executed their additional role to enhance the chaperon activity of HAA by a positive cooperative effect. Therefore, it is expected that the improvement of the complexing ability of Schiff bases can make it a more potent inhibitor against Cu^{2+}-mediated aggregation of β- and γ-crystallins. This particular approach can be further developed as a potential alternative to conventional cataract treatment.

Acknowledgements KSG is grateful to Science and Engineering Research Board (SERB) under Department of Science and Technology (DST), Govt. of India, for funding through its sanctioned project (No. SB/FT/LS-277/2012). JD is grateful to DST (SB/FT/CS-008/2013), New Delhi, India, for financial support. AB thanks DST for a fellowship. JD is thankful to CARISM and CRF, SASTRA University, for availing their 300 MHz NMR and UV–Vis spectrophotometer. PC and KSG are thankful to CMSE, NIT Hamirpur, for providing some of the instrumentation facilities. KSG is also grateful to Prof. D. Balasubramanian, L.V. Prasad Eye Hospital, Hyderabad, and Prof. K.P. Das, Bose Institute, Kolkata, for proving the clones of HGD and HAA, respectively.

References

1. Miller LM, Wang Q, Telivala TP, Smith RJ, Lanzirotti A, Miklossy J (2006) Synchrotron-based infrared and X-ray imaging shows focalized accumulation of Cu and Zn co-localized with β-amyloid deposits in Alzheimer's disease. J Struct Biol 15:530–537
2. Gaggelli E, Kozlowski H, Valensin D, Valensin G (2006) Copper homeostasis and neurodegenerative disorders (Alzheimer's, prion, and Parkinson's diseases and amyotrophic lateral sclerosis). Chem Rev 106:1995–2044
3. Davies KM, Bohic S, Carmona A, Ortega R, Cottam V, Hare DJ, Finberg JPM, Reyes S, Halliday GM, Mercer JFB, Double KL

(2014) Copper pathology in vulnerable brain regions in Parkinson's disease. Neurobiol Aging 35:858–866
4. Bonda DJ, Lee HG, Blair JA, Zhu X, Perry G, Smith MA (2011) Role of metal dyshomeostasis in Alzheimer disease. Metallomics 3:267–270
5. Hureau C, Faller P (2009) Aβ-mediated ROS production by Cu ions: structural insights, mechanisms and relevance to Alzheimer's disease. Biochimie 91:1212–1217
6. Mayes J, Mill CT, Kolosov O, Zhang H, Tabner BJ, Allsop D (2014) β-amyloid fibrils in Alzheimer's disease are not inert when bound to copper ions but can degrade hydrogen peroxide and generate reactive oxygen species. J Biol Chem 289:12052–12062
7. Zhu X, Su B, Wang X, Smith MA, Perry G (2007) Causes of oxidative stress in Alzheimer disease cell. Mol Life Sci 64:2202–2210
8. Eskici G, Axelsen PH (2012) Copper and oxidative stress in the pathogenesis of Alzheimer's disease. Biochemistry 51:6289–6311
9. Garland D (1990) Role of site-specific, metal-catalyzed oxidation in lens aging and cataract: a hypothesis. Exp Eye Res 50:677–682
10. Atalay A, Ogus A, Bateman O, Slingsby C (1998) Vitamin C induced oxidation of eye lens gamma crystallins. Biochimie 80:283–288
11. Garner B, Roberg K, Qian M, Brunk UT, Eaton JW, Truscott RJW (1999) Redox availability of lens iron and copper: implications for $HO^{\cdot}$ generation in cataract. Redox Rep 4:313–315
12. Padgaonkar VA, Leverenz VR, Fowler KE, Reddy VN (2000) The effects of hyperbaric oxygen on the crystallins of cultured rabbit lenses: a possible catalytic role for copper. Exp Eye Res 71:371–383
13. Ortwerth BJ, James HL (1999) Lens proteins block the copper-mediated formation of reactive oxygen species during glycation reactions in vitro. Biochem Biophys Res Commun 259:706–710
14. Ahmad MF, Singh D, Taiyab A, Ramakrishna T, Raman B, Rao CM (2008) Selective Cu^{2+} binding, redox silencing, and cytoprotective effects of the small heat shock proteins αA- and αB-crystallin. J Mol Biol 38:2812–2824
15. Ganadu ML, Aru M, Mura GM, Coi A, Mlynarz P, Kozlowski H (2004) Effects of divalent metal ions on the alphaB-crystallin chaperone-like activity: spectroscopic evidence for a complex between copper (II) and protein. J Inorg Biochem 98:1103–1109
16. Biswas A, Das KP (2008) Zn^{2+} enhances the molecular chaperone function and stability of alpha-crystallin. Biochemistry 47:804–816
17. Horwitz J (1992) α-Crystallin can function as a molecular chaperone. Proc Natl Acad Sci 89:10449–10453
18. Sampson LA, King J (2010) Partially folded aggregation intermediates of human γD-, γC-, and γS-crystallin are recognized and bound by human αB-crystallin chaperone. J Mol Biol 401:134–152
19. Ghosh KS, Pande A, Pande J (2011) Binding of γ-crystallin substrate prevents the binding of copper and zinc ions to the molecular chaperone α-crystallin. Biochemistry 50:3279–3281
20. Rasi V, Costantini S, Moramarco A, Giordano R, Giustolisi R, Gabrieli CB (1992) Inorganic element concentrations in cataractous human lenses. Ann Ophthalmol 24:459–464
21. Srivastava VK, Varshney N, Pandey DC (1992) Role of trace elements in senile cataract. Acta Ophthalmol 70:839–841
22. Cekic O (1998) Effect of cigarette smoking on copper, lead, and cadmium accumulation in human lens. Br J Ophthalmol 82:186–188
23. Quintanar L, Domínguez-Calva JA, Serebryany E, Rivillas-Acevedo L, Haase-Pettingell C, Amero C, King JA (2016) Copper and zinc ions specifically promote nonamyloid aggregation of the highly stable human γ-D crystallin. ACS Chem Biol 11:263–272
24. Grossi C, Francese S, Casini A, Rosi MC, Luccarini I, Fiorentini A, Gabbiani C, Messori L, Moneti G, Casamenti F (2009) Clioquinol decreases amyloid-β burden and reduces working memory impairment in a transgenic mouse model of Alzheimer's disease. J Alzheimers Dis 17:423–440
25. Greenough MA, Camakaris J, Bush AI (2013) Metal dyshomeostasis and oxidative stress in Alzheimer's disease. Neurochem Int 62:540–555
26. Oliveri V, Attanasio F, Puglisi A, Spencer J, Sgarlata C, Vecchio G (2014) Multifunctional 8-hydroxyquinoline-appended cyclodextrins as new inhibitors of metal-induced protein aggregation. Chem Eur J 20:8954–8964
27. Choi J, Braymer JJ, Nanga RPR, Ramamoorthy A, Lim MH (2010) Design of small molecules that target metal-Aβ species and regulate metal-induced Aβ aggregation and neurotoxicity. Proc Natl Acad Sci 107:21990–21995
28. Sharma AK, Pavlova ST, Kim J, Finkelstein D, Hawco NJ, Rath NP, Kim J, Mirica LM (2012) Bifunctional compounds for controlling metal-mediated aggregation of the Aβ42 peptide. J Am Chem Soc 134:6625–6636
29. Gomes LMF, Vieira RP, Jones MR, Wang MCP, Dyrager C, Souza-Fagundes EM, Da JG, SilvaStorr T, Beraldo H (2014) 8-hydroxyquinoline Schiff-base compounds as antioxidants and modulators of copper-mediated Aβ peptide aggregation. J Inorg Biochem 139:106–116
30. Bareggi SR, Cornelli U (2012) Clioquinol: review of its mechanisms of action and clinical uses in neurodegenerative disorders. CNS Neurosci Ther 18:41–46
31. Cherny RA, Ayton S, Finkelstein DI, Bush AI, McColl G, Massa SM (2012) PBT2 reduces toxicity in a *C. elegans* model of polyQ aggregation and extends lifespan, reduces striatal atrophy and improves motor performance in the R6/2 mouse model of Huntington's disease. J Huntingtons Dis 1:211–219
32. Kumar BD, Rawat DS (2013) Synthesis and antioxidant activity of thymol and carvacrol based Schiff bases. Bioorg Med Chem Lett 23:641–645
33. Li C, Xu X, Wang XJ, Pan Y (2014) Imine resveratrol analogues: molecular design, Nrf2 activation and SAR analysis. PLoS One 9:e101455
34. Huber D, Andermann G, Leclerc G (1988) Selective reduction of aromatic/aliphatic nitro groups by sodium sulfide. Tetrahedron Lett 29:635–638
35. Leleu S, Papamicae C, Marsais F, Dupas G, Levacher V (2004) Preparation of axially chiral quinolinium salts related to NAD+ models: new investigations of these biomimetic models as 'chiral amide-transferring agents. Tetrahedron Asymmetry 15:3919–3928
36. Benesi HA, Hildebrand JH (1949) A spectrophotometric investigation of the interaction of iodine with aromatic hydrocarbons. J Am Chem Soc 71:2703–2707
37. Kao S, Lin W, Venkatesan P, Wu S (2014) Colorimetric detection of Cu(II): Cu(II)-induced deprotonation of NH responsible for color change. Sens Actuators B 204:688–693
38. Kim KB, Park GJ, Kim H, Song EJ, Bae JM, Kim C (2014) A novel colorimetric chemosensor for multiple target ions in aqueous solution: simultaneous detection of Mn(II) and Fe(II). Inorg Chem Commun 46:237–240
39. Goswami S, Aich K, Das S, Das AK, Manna A, Halder S (2013) A highly selective and sensitive probe for colorimetric and fluorogenic detection of Cd^{2+} in aqueous media. Analyst 138:1903–1907
40. Ghule NV, Bhosale RS, Puyad AL, Bhosale SV, Bhosale SV (2016) Naphthalenediimide amphiphile based colorimetric

probe for recognition of Cu^{2+} and Fe^{3+} ions. Sens Actuators B 227:17–23
41. Frisch MJ et al (2009) Gaussian 03, revision D.02. Gaussian, Inc., Pittsburgh
42. Shimada K, Fujikawa K, Yahara K, Nakamura T (1992) Antioxidative properties of xanthan on the autooxidation of soybean oil in cyclodextrin emulsion. J Agric Food Chem 40:945–948
43. Pande A, Pande J, Asherie N, Lomakin A, Ogun O, King JA, Lubsen NH, Walton D, Benedek GB (2000) Molecular basis of a progressive juvenile-onset hereditary cataract. Proc Natl Acad Sci 97:1993–1998
44. Andley UP, Mathur S, Griest TA, Petrash JM (1996) Cloning, expression, and chaperone like activity of human alphaA-crystallin. J Biol Chem 271:31973–31980
45. Horwitz J, Huang QL, Ding L, Bova MP (1998) Lens alpha-crystallin: chaperone-like properties. Methods Enzymol 290:365–383
46. Spector A (1964) Methods of isolation of alpha, beta, and gamma crystallins and their subgroups. Invest Ophthalmol 3:182–193
47. Wu G, Wang G, Fu X, Zhu L (2003) Synthesis, crystal structure, stacking effect and antibacterial studies of a novel quaternary copper (II) complex with quinolone. Molecules 8:287–296
48. Wright JS, Johnson ER, DiLabio GA (2001) Predicting the activity of phenolic antioxidants: theoretical method, analysis of substituent effects, and application to major families of antioxidants. J Am Chem Soc 123:1173–1183
49. Chen W, Guo P, Song J, Cao W, Bian J (2006) The ortho hydroxy-amino group: another choice for synthesizing novel antioxidants. Bioorg Med Chem Lett 16:3582–3585
50. Bendary E, Francis RR, Ali HMG, Sarwat MI, Hady SE (2013) Antioxidant and structure–activity relationships (SARs) of some phenolic and anilines compounds. Ann Agric Sci 58:173–181
51. Ordoudi SA, Tsimidou MZ, Vafiadis AP, BakalBassis EG (2006) Structure-DPPH. Scavenging activity relationships: parallel study of catechol and guaiacol acid derivatives. J Agric Food Chem 54:5763–5768
52. Valgimigli L, Amorati R, Fumo MG, Dilabio GA, Pedulli GF, Ingold KU, Pratt DA (2008) The unusual reaction of semiquinone radicals with molecular oxygen. J Org Chem 73:1830–1841